J. Appl. Comput. Mech., 7(4) (2021) 1892–1906
DOI: 10.22055/JACM.2019.31060.1822

ISSN: 2383-4536
jacm.scu.ac.ir

Shahid Chamran University of Ahvaz

Journal of Applied and Computational Mechanics

Research Paper

Effects of Inclined Magnetic Field and Porous Medium on Peristaltic Flow of a Bingham Fluid with Heat Transfer

B.B. Divya[1], G. Manjunatha[2], C. Rajashekhar[3], H. Vaidya[4], K.V. Prasad[5]

[1] Department of Mathematics, Manipal Institute of Technology, Manipal Academy of Higher Education, Manipal, Karnataka, 576104, India, Email: divyabaliga2711@gmail.com

[2] Department of Mathematics, Manipal Institute of Technology, Manipal Academy of Higher Education, Manipal, Karnataka, 576104, India, Email: gudekote_m@rediffmail.com

[3] Bhaskaracharya Study Chair, Karnataka State Akkamahadevi Women's University, Vijayapura, Karnataka, 586108, India, Email: choudhariraj3@gmail.com

[4] Department of Mathematics, Vijayanagara Srikrishnadevaraya University, Ballari, Karnataka, 583105, India, Email: hanumeshvaidya@gmail.com

[5] Department of Mathematics, Vijayanagara Srikrishnadevaraya University, Ballari, Karnataka, 583105, India, Email: prasadkv2007@gmail.com

Received September 13 2019; Revised November 07 2019; Accepted for publication November 26 2019.
Corresponding author: G. Manjunatha (gudekote_m@rediffmail.com)

Abstract. The current paper aims to explain the peristaltic mechanism of a Bingham fluid with varying viscosity. The fluid is considered to flow within a porous medium and subjected to a magnetic field with significant inclination. Heat transfer characteristics are studied with convective conditions and variable thermal conductivity. The solution is obtained by the perturbation technique, where small values of variable liquid properties are utilized. The graphs plotted indicate that variation in viscosity as well as thermal conductivity actively contribute to reduce the pressure gradient. Further, for a higher radius of the plug flow region, a higher pressure rise occurs. The magnetic parameter and Grashof number influence the trapping phenomenon by reducing the dimensions of the bolus.

Keywords: Biot number, Darcy number, Grashof number, Inclined magnetic field, Plug flow.

1. Introduction

In the span of research concerning fluids, the peristaltic mechanism is well-studied owing to multiple applications in physiological as well as industrial fields. Peristalsis facilitates the flow of fluid within the corresponding system through a progressive expanding and contracting wave, moving along the tube/channel carrying the fluid. Within biological systems, peristalsis is responsible for phenomena including but not limited to the movement of food particles within the esophagus, motion of chyme within the intestine and other such biological processes. Initial investigations focusing on peristaltic transport have considered the Newtonian fluid model to hold true. However, subsequent research has proven that a majority of physiological fluids exhibit non-Newtonian behavior, which has led to a re-examination of the peristaltic mechanism with non-Newtonian considerations. One of the first investigations on this front was conducted by Srivastava and Srivastava [1], who considered a power-law model to study the peristalsis through both uniform as well as non-uniform channels. Two-layer fluid models have been studied by Narahari and Sreenadh [2] in their attempt to investigate the peristaltic mechanism of a Newtonian fluid in contact with a Bingham fluid. In order to analyze the flow behavior in the unyielded plug region, Frigaard and Ryan [3] developed an asymptotic solution for the Poiseuille flow of Bingham fluid through a two-dimensional channel with very small variations in width. An in-depth study on Bingham fluid flow was carried out by Fusi [4] in which the yield stress and viscosity were considered to be dependent on pressure as well as temperature. The influence of heat during peristaltic mechanism is an important component of research in multiple applications, some of which include blood pumps within heart lung machines, transport of sanitary fluid and the movement of corrosive fluids without contact with the machinery parts. Thus, while studying peristalsis, especially within biological systems, it is important to take heat transfer effects into account. To that end, many studies on peristalsis have been conducted on non-Newtonian fluids with heat transfer considerations. Recently, Vaidya et al. [5] formulated the effects of the transfer of heat on peristalsis for a Bingham fluid. They also investigated the heat transfer of a Rabinowitsch fluid flowing through a complaint channel with porous walls [6]. Several investigations have been carried out for heat transfer mechanisms with various configurations and flow geometries [7-9].

With recent developments in science and technology, biological systems are increasingly being exposed to various magnetic fields. In order to set exposure limits for these technologies, it becomes imperative to review the effects of magnetic field on physiological processes. Erythrocytes, a major constituent of blood, are known to exhibit biomagnetic properties and thus, magnetic fields are proven to have a substantial effect on peristaltic transport of blood. For this reason, attempts have been made to explain the peristalsis of fluid when exposed to magnetic fields. The effect of a magnetic field, applied with ion and hall slip, on the peristaltic mechanism of an electrically conducting hyperbolic tangent fluid was researched by Abdelsalam et al. [10]. From the study, it could be inferred that the slip and hall parameters play a major role in boosting the velocity before a critical point. Akram

Published online: March 26 2020

et al. [11], in their heat and mass transfer studies on Bingham fluid, considered a magnetic field with inclination. Sinha et al. [12] studied the peristaltic mechanism of a magnetohydrodynamic (MHD) fluid within an asymmetric channel. In addition to the magnetohydrodynamic studies, ferromagnetic studies are also found to have wide applications in industries. Inspired by this, Akbar et al. [13, 14] have extensively studied the peristalsis of nanofluid models with heat transfer characteristics. In the recent past, many such studies have been done on peristaltic mechanism to investigate the effects of magnetic field for various fluid model configurations [15-21].

Another consideration of equal importance, especially for biological systems, is the permeability of the medium of transport. Investigations have been conducted on peristaltic mechanism within a porous medium by Kothandapani and Srinivas [22] to study the impact of elastic properties of the wall on peristalsis of an MHD fluid with heat transfer considerations. Taking porous medium into account, Srinivas et al. elucidated on the peristalsis in a rigid asymmetric vertical channel [23] and the impact of wall characteristics and heat transfer on peristalsis [24]. Further, Eldesoky et al. [25] carried out theoretical investigations on the magnetohydrodynamics and heat transfer mechanism of peristaltic motion of a particle-fluid suspension through a porous channel. In their studies, the temperature was found to rise with Reynolds number irrespective of the presence or absence of suspension. These studies considered the Newtonian fluid model. However, investigations in this dimension have also extended to cover non-Newtonian fluid behavior. Ramesh and Devakar [26] investigated a couple stress fluid undergoing peristalsis under the influence of magnetic field in an asymmetric channel. Mahmoud et al. [27] investigated the impact of magnetism and porous medium on the movement of a Jeffrey fluid. While Rathod and Laxmi [28] elucidated on the impact of transfer of heat on the flow of an MHD Bingham fluid within porous medium, Laxminarayana et al. [29] extended upon the study to assess the impact of slip and wall characteristics on the peristalsis of a conducting Bingham fluid. Several investigations were carried out to analyze the impact of porous medium on the non-Newtonian flow through different geometries [30-33].

Investigations conducted to explain the flow of blood within biological systems must take into account the variation in its viscosity. This is because the viscosity of blood has been observed to vary with the thickness of the conducting arteries. Specifically, the viscosity of the blood flowing close to the periphery is found to be lower than that of the blood flowing close to the centre. Experiments to investigate the impact of variable viscosity have been conducted with both Newtonian [34] and non-Newtonian [35] fluid model considerations. Fusi et al. [36] carried out rigorous studies on a bi-viscous model and showed that Bingham model is ultimately obtained from the bi-viscous model when one viscosity tends to infinity and the other is bounded. In addition to variable viscosity, blood has also shown to exhibit variable thermal conductivity depending on the temperature. Studies considering both variable viscosity as well as thermal conductivity has been conducted for non-Newtonian fluid models. Models investigated include Bingham [37], Rabinowitsch [38] and Jeffrey [39] fluid models.

In the present paper, the authors have attempted to explain peristalsis for a Bingham fluid through the length of a channel with significant inclination and porous medium considerations. During the investigation, the impact of transfer of heat with convective boundary conditions has been taken into account. The conducting fluid is considered to show variable thermal conductivity as well as variable viscosity. Additionally, to investigate the impact of exposure to magnetic field, MHD fluid flow assumptions have been considered. The magnetic field under consideration is assumed to be inclined. The obtained perturbed solution to the system is graphed and the impact of relevant parameters have been discussed. In the course of our research, we have found that no work has been reported yet that considers the variable viscosity and thermal conductivity of a peristaltically induced Bingham fluid motion through a porous media under the impact of a magnetic field with inclination.

2. Formulation of the Problem

In order to formulate the problem, the electrically conducting Bingham fluid is considered to flow in a two-dimensional channel with porous medium. The peristaltic wave train, moving at a uniform speed c, induces the flow of the fluid. The fluid motion is also considered to be subjected to a magnetic field with magnitude denoted by B_0 in the transverse direction. An inclination of γ and ϕ is considered for the channel and magnetic field respectively. The channel is considered to be symmetric about the axis. Moreover, as the Reynolds number is considered to be very small, it makes it possible for us to neglect the induced magnetic field. The plug flow region refers to the portion of the channel between the axis $y = 0$ and $y = y_p$, where $|\tau_{xy}| \le \tau_0$. For the region encapsulated by y_p and H', $|\tau_{xy}| > \tau_0$. The problem is modelled as shown in Fig. 1. The deformation in the channel walls due to the peristaltic waves is given by:

$$H'(X,t) = a' + b'\sin\left[\frac{2\pi}{\lambda}(X - ct)\right] \tag{1}$$

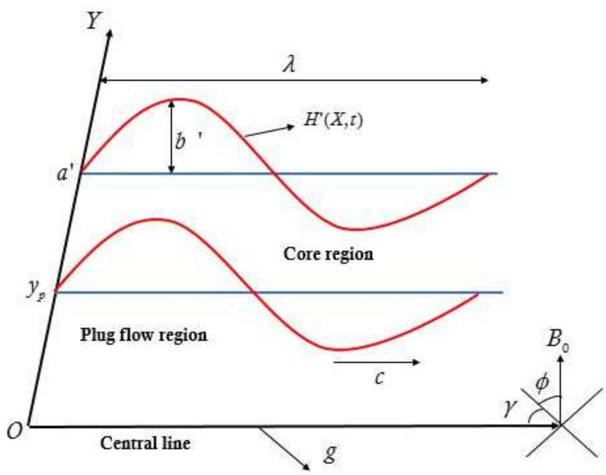

Fig. 1. Geometry of the problem.

The flow is unsteady in the laboratory frame (X, Y). Thus, with the assumptions of constant pressure difference across the channel ends and that the channel length is an integral multiple of the wavelength λ, the flow becomes steady in the wave frame of reference (x, y). The wave frame is moving away from the fixed frame at a constant speed c. The transformations between these two frames is as follows:

$$x = X - ct, y = Y, w = W - c, v = V \text{ and } p(x,y) = P(X,Y,t). \tag{2}$$

where W, w are the axial velocity component in the laboratory and wave frames respectively, V and v are the components of velocity in the transverse direction in the fixed and wave frames respectively. The equations which govern the fluid flow in the wave frame are given by

$$\frac{\partial w}{\partial x} + \frac{\partial v}{\partial y} = 0, \tag{3}$$

$$\rho\left(w\frac{\partial w}{\partial x} + v\frac{\partial w}{\partial y}\right) = -\frac{\partial p}{\partial x} + \frac{\partial \tau_{xx}}{\partial x} + \frac{\partial \tau_{xy}}{\partial y} - \sigma B_0^2 \cos\phi((w+c)\cos\phi - v\sin\phi) - \frac{\mu}{k}(w+c) + \rho g \beta' \sin\gamma(T - T_0), \tag{4}$$

$$\rho\left(w\frac{\partial w}{\partial x} + v\frac{\partial w}{\partial y}\right) = -\frac{\partial p}{\partial y} + \frac{\partial \tau_{xy}}{\partial x} + \frac{\partial \tau_{yy}}{\partial y} + \sigma B_0^2 \sin\phi((w+c)\cos\phi - v\sin\phi) - \frac{\mu}{k}v + \rho g \beta' \cos\gamma(T - T_0), \tag{5}$$

$$\rho C_p\left(w\frac{\partial T}{\partial x} + v\frac{\partial T}{\partial y}\right) = k^*\left[\frac{\partial}{\partial x}\left(k(T)\frac{\partial T}{\partial x}\right) + \frac{\partial}{\partial y}\left(k(T)\frac{\partial T}{\partial y}\right)\right] + Q_0. \tag{6}$$

in which τ_{ij} represents the stress tensors of the Bingham fluid given by [28]:

$$\tau_{ij} = \left(\mu + \frac{\tau_0}{\dot{\gamma}}\right)\dot{\gamma}_{ij}, \text{ for } \tau \ge \tau_0, \tag{7}$$

$$\tau_{ij} = \dot{\gamma}_{ij} = 0, \text{ for } \tau < \tau_0, \tag{8}$$

where the rate of strain tensor $\dot{\gamma}_{ij}$ is

$$\dot{\gamma}_{ij} = \frac{\partial w_i}{\partial x_j} + \frac{\partial w_j}{\partial x_i}, \tag{9}$$

$$\tau = \sqrt{\frac{1}{2}\tau_{ij}^2}, \tag{10}$$

$$\dot{\gamma}_{ij} = \sqrt{\frac{1}{2}\dot{\gamma}_{ij}^2} = \sqrt{\left(\frac{\partial w}{\partial x}\right)^2 + \left(\frac{\partial v}{\partial y}\right)^2 + \left(\frac{\partial w}{\partial y} + \frac{\partial v}{\partial x}\right)^2}, \tag{11}$$

and

$$\mu = \mu(y) = e^{-\xi_1 y} = 1 - \xi_1 y + O\left(\xi_1^{\,2}\right) \tag{12}$$

is the variable viscosity with the variable viscosity coefficient $\xi_1 << 1$. We now use the following non-dimensional quantities:

$$\begin{gathered} x^* = \frac{x}{\lambda}, y^* = \frac{y}{a'}, w^* = \frac{w}{c}, v^* = \frac{v}{c\delta}, t^* = \frac{ct}{\lambda}, h = \frac{H'}{a'}, \tau_y = \frac{a'}{\lambda}\tau_y{}', \delta = \frac{a'}{\lambda}, \varepsilon = \frac{b'}{a'}, Re = \frac{\rho c a'}{\mu}, \theta = \frac{T - T_0}{T_1 - T_0}, p' = \frac{a'^2}{c\lambda\mu}p, y_p^* = \frac{y_p}{a'}, \\ \beta = \frac{Q_0 a'^2}{k^*(T_1 - T_0)}, Da = \frac{k}{a'^2}, Pr = \frac{\mu C_p}{k^*}, Gr = \frac{\rho\beta' g a'^2(T_1 - T_0)}{\mu c}, M = \sqrt{\frac{\sigma}{\mu}}B_0 a'. \end{gathered} \tag{13}$$

Incorporating the above quantities into Eqs. (3)-(6), we obtain (after dropping the asterisks),

$$\frac{\partial w}{\partial x} + \frac{\partial v}{\partial y} = 0, \tag{14}$$

$$Re\,\delta\left(w\frac{\partial w}{\partial x} + v\frac{\partial w}{\partial y}\right) = -\frac{\partial p}{\partial x} + \delta^2\frac{\partial \tau_{xx}}{\partial x} + \frac{\partial \tau_{xy}}{\partial y} - \left(M^2\cos^2\phi + \frac{1}{Da}\right)(w+1) + M^2 v\delta\sin\phi\cos\phi + Gr\,\theta\sin\gamma, \tag{15}$$

$$Re\,\delta^3\left(w\frac{\partial w}{\partial x} + v\frac{\partial w}{\partial y}\right) = -\frac{\partial p}{\partial y} + \delta^2\frac{\partial \tau_{xy}}{\partial x} + \delta\frac{\partial \tau_{yy}}{\partial y} - \frac{\delta^2}{Da}v + \delta Gr\,\theta\cos\gamma + M^2\delta\sin\phi((w+1)\cos\phi - v\delta\sin\phi), \tag{16}$$

$$Re\,Pr\,\delta\left(w\frac{\partial\theta}{\partial x}+v\frac{\partial\theta}{\partial y}\right)=\delta^2\frac{\partial}{\partial x}\left(k(\theta)\frac{\partial\theta}{\partial x}\right)+\frac{\partial}{\partial y}\left(k(\theta)\frac{\partial\theta}{\partial y}\right)+Q_0, \tag{17}$$

where

$$\tau_{ij}=\left(\mu+\frac{\tau_0}{\dot{\gamma}}\right)\dot{\gamma}_{ij}\text{ for }\tau\geq\tau_0, \tag{18}$$

$$\tau_{ij}=\dot{\gamma}_{ij}=0\text{ for }\tau<\tau_0, \tag{19}$$

$$\dot{\gamma}_{xy}=\dot{\gamma}_{yx}=\frac{\partial w}{\partial y}+\delta^2\frac{\partial w}{\partial x}, \tag{20}$$

$$\dot{\gamma}_{xx}=2\delta\frac{\partial w}{\partial x},\dot{\gamma}_{yy}=2\delta\frac{\partial v}{\partial y}, \tag{21}$$

$$\dot{\gamma}=\sqrt{2\delta^2\left[\left(\frac{\partial w}{\partial x}\right)^2+\left(\frac{\partial v}{\partial y}\right)^2\right]+\left(\frac{\partial w}{\partial y}+\delta^2\frac{\partial v}{\partial y}\right)^2}, \tag{22}$$

$$\tau=\sqrt{\tau_{xy}^2+\tau_{xx}^2}. \tag{23}$$

By considering the assumptions of long wavelength and low Reynolds number approximations, Eqs. (14)-(16) become

$$\frac{\partial p}{\partial y}=0, \tag{24}$$

$$\frac{\partial p}{\partial x}=\frac{\partial\tau_{xy}}{\partial y}-\left(M^2\cos^2\phi+\frac{1}{Da}\right)(w+1)+Gr\theta\sin\gamma, \tag{25}$$

$$\frac{\partial}{\partial y}\left[k(\theta)\frac{\partial\theta}{\partial y}\right]+\beta=0, \tag{26}$$

with the variable thermal conductivity

$$k(\theta)=e^{\xi_2\theta}=1+\xi_2\theta+O\left(\xi_2^2\right), \tag{27}$$

where $\xi_2<<1$ being the coefficient of variable thermal conductivity. The non-dimensional constitutive equation of Bingham fluid is given by

$$\tau_{xy}=\mu(y)\left(-\frac{\partial w}{\partial y}\right)-\tau_0\text{ for }\tau\geq\tau_0, \tag{28}$$

$$\tau_{xy}=0\text{ for }\tau<\tau_0. \tag{29}$$

The boundary conditions in the non-dimensional form are

$$\frac{\partial w}{\partial y}=\tau_0\text{ at }y=0,w=-1\text{ at }y=h=1+\varepsilon\left[2\pi(x-t)\right], \tag{30}$$

$$\frac{\partial\theta}{\partial y}=0\text{ at }y=0,\frac{\partial\theta}{\partial y}+Bi\theta=0\text{ at }y=h. \tag{31}$$

The volume flux through each cross-section of the channel in the wave frame is

$$q=\int_0^{y_p}w_p\,dy+\int_{y_p}^{h}w\,dy. \tag{32}$$

The instantaneous volume flow rate in the laboratory frame between the channel center and the wall is given by

$$Q(X,t)=\int_0^{H'}W\,dy=\int_0^{h}(w+1)dy=q+h. \tag{33}$$

3. Perturbation Solution to the Problem

The solution to temperature equation given by Eq. (26) along with the boundary conditions (Eq. (31)) is obtained by the perturbation method up to the first order for small values of ξ_2 as

$$\theta = -\beta\frac{y^2}{2} + c_2 + \frac{\xi_2}{2}\left[2c_3 - \left(c_2 - \frac{\beta y^2}{2}\right)^2\right]. \tag{34}$$

The solution for Eq. (25) with the boundary conditions given by eq. (30) is found by the perturbation solution up to the first order for small values of ξ_1 as

Zeroth Order Solution:

$$w_0 = c_4\cos Ey + c_5\sin Ey - \frac{(P+E^2)}{E^2} + \frac{Gr\sin\gamma}{E^2}\left[c_6 + \beta\left(c_7 + c_8y^2 - \frac{\xi_2\beta}{8}\left(y^4 - \frac{12y^2}{E^2} + \frac{24}{E^4}\right)\right)\right]. \tag{35}$$

First Order Solution:

$$w_1 = c_9\cos Ey + c_{10}\sin Ey + \frac{Ey^2}{4}(c_5\cos Ey - c_4\sin Ey) + \frac{y}{4}(c_5\sin Ey + c_4\cos Ey) + \frac{Gr\beta\sin\gamma}{E^4}\left(4c_8y + \frac{18\xi_2\beta y}{E^2} - 2\xi_2\beta y^3\right), \tag{36a}$$

where

$$P = \frac{dp}{dx}, E^2 = M^2\cos^2\phi + \frac{1}{Da}. \tag{36b}$$

Hence, we obtain the solution for velocity in the axial direction as

$$w = w_0 + \xi_1 w_1. \tag{37}$$

Having the velocity expression, we now find the upper limit of the plug flow region with the help of the following boundary condition:

$$\frac{\partial w}{\partial y} = 0 \text{ at } y = y_p. \tag{38}$$

Using the above condition, we obtain

$$\tau_0 = \frac{P\sec Eh\left[E\sin Ey_p\left(1 + \frac{3\xi_1 y_p}{4}\right) - \frac{\cos Ey_p}{4}\left(\xi_1 - \xi_1E^2y_p^2\right)\right]}{E^2\left(c_{15}\sin Ey_p + c_{16}\cos Ey_p\right)} + c_{18}. \tag{39}$$

Considering $y = y_p$ in Eq. (37), we get the plug flow velocity as

$$w_p = \frac{Gr\sin\gamma}{E^2}\left[c_6 + \beta\left(c_7 + c_8y_p^2 - \xi_2c_{21} + \xi_1c_{22}\right)\right] + c_{19}\cos Ey_p + c_{20}\sin Ey_p - 1 - \frac{P}{E^2}. \tag{40}$$

The volume flux through each cross-section in the wave frame is

$$\begin{aligned} q = \int_0^{y_p} w_p\,dy + \int_{y_p}^{h} w\,dy &= -h + c_{27}y_p\cos Ey_p + c_{30}y_p\sin Ey_p + c_{39}\sin E(h-y_p) + c_{44}\cos E(h-y_p) + c_{45} + P\left[\frac{-h}{E^2} + c_{26}y_p\cos Ey_p\right. \\ &\left. + c_{29}y_p\sin Ey_p + c_{38}\sin E(h-y_p) + c_{43}\cos E(h-y_p)\right]. \end{aligned} \tag{41}$$

Rearranging the terms in the above, we obtain

$$P = \frac{dp}{dx} = \frac{q + h - c_{27}y_p\cos Ey_p - c_{30}y_p\sin Ey_p - c_{39}\sin E(h-y_p) - c_{44}\cos E(h-y_p) - c_{45}}{\frac{-h}{E^2} + c_{26}y_p\cos Ey_p + c_{29}y_p\sin Ey_p + c_{38}\sin E(h-y_p) + c_{43}\cos E(h-y_p)}. \tag{42}$$

We have the relationship between the stream function and axial velocity as

$$w = \frac{\partial\psi}{\partial y}, v = -\frac{\partial\psi}{\partial x}, \tag{43a}$$

and the boundary condition is

$$\psi = 0 \text{ at } y = 0. \tag{43b}$$

Using the above, the stream function is obtained as

$$\begin{aligned} \psi = c_4\frac{\sin Ey}{E} - c_5\frac{\cos Ey}{E} + \frac{Gr\sin\gamma}{E^2}\left[c_6y + \beta\left(c_7y + c_8\frac{y^3}{3} - \frac{\xi_2\beta}{8}\left(\frac{y^5}{5} - \frac{4y^3}{E^2} + \frac{24y}{E^4}\right)\right)\right] + \xi_1\left[c_9\frac{\sin Ey}{E} - c_{10}\frac{\cos Ey}{E} + \right. \\ c_5\left(y^2\frac{\sin Ey}{4} + \frac{y\cos Ey}{4E} - \frac{\sin Ey}{4E^2}\right) + c_4\left(\frac{y^2\cos Ey}{4} - \frac{y\sin Ey}{4E} - \frac{\cos Ey}{4E^2}\right) + \left.\frac{Gr\beta\sin\gamma}{E^4}\left(2c_8y^2 + \frac{9\xi_2\beta y^2}{E^2} - \frac{\xi_2\beta y^4}{2}\right)\right] \end{aligned} \tag{44}$$

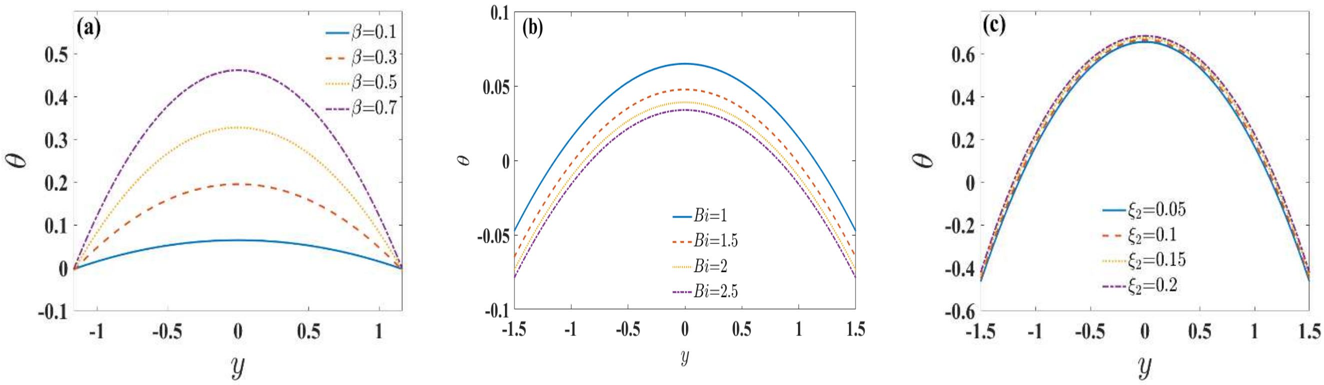

Fig. 2. Temperature profiles for different values of (a) β , (b) Bi and (c) ξ_2.

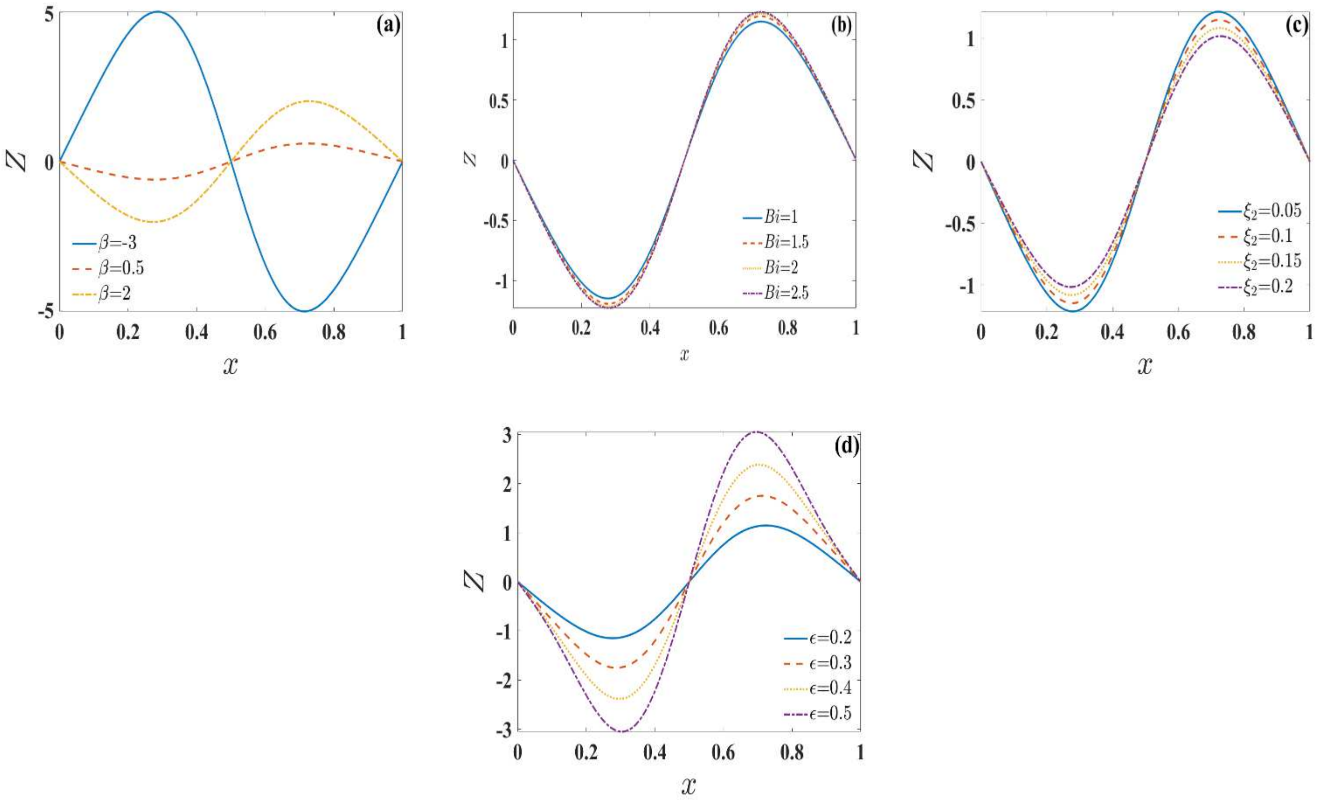

Fig. 3. Heat transfer coefficient for different values of (a) β , (b) Bi, (c) ξ_2 and (d) ε .

The pressure rise and frictional force over one wavelength is given by

$$\Delta p = \int_0^1 \frac{dp}{dx} dx, \tag{45a}$$

$$F = -\int_0^1 h \frac{dp}{dx} dx. \tag{45b}$$

The above integrals are calculated numerically and graphed using MATLAB.

4. Results and Discussion

In the present section, we attempt to explain the influence of important parameters on temperature profiles, coefficient of heat transfer, pressure gradient, pressure rise, frictional force and streamline patterns for the trapping phenomenon. Graphical representations through MATLAB are presented to observe the behavioral patterns. The physical parameters of interest are Hartmann number (M), Darcy number (Da), heat generation parameter (β) , variable thermal conductivity (ξ_2), Biot number (Bi), variable viscosity (ξ_1) , inclination of the magnetic field (ϕ) , plug flow radius (y_p), Grashof number (Gr) and angle of inclination of the channel (γ) . The values of the fixed parameters are:

$$t = 0.25,\ x = 0.1,\ \varepsilon = 0.1,\ \beta = 1,\ Bi = 1,\ \xi_2 = 0.1,\ M = 2,\ \phi = \frac{\pi}{6},\ Da = 0.5,\ y_p = 0.2,\ Gr = 3,\ \gamma = \frac{\pi}{6} \text{ and } \xi_1 = 0.1. \tag{46}$$

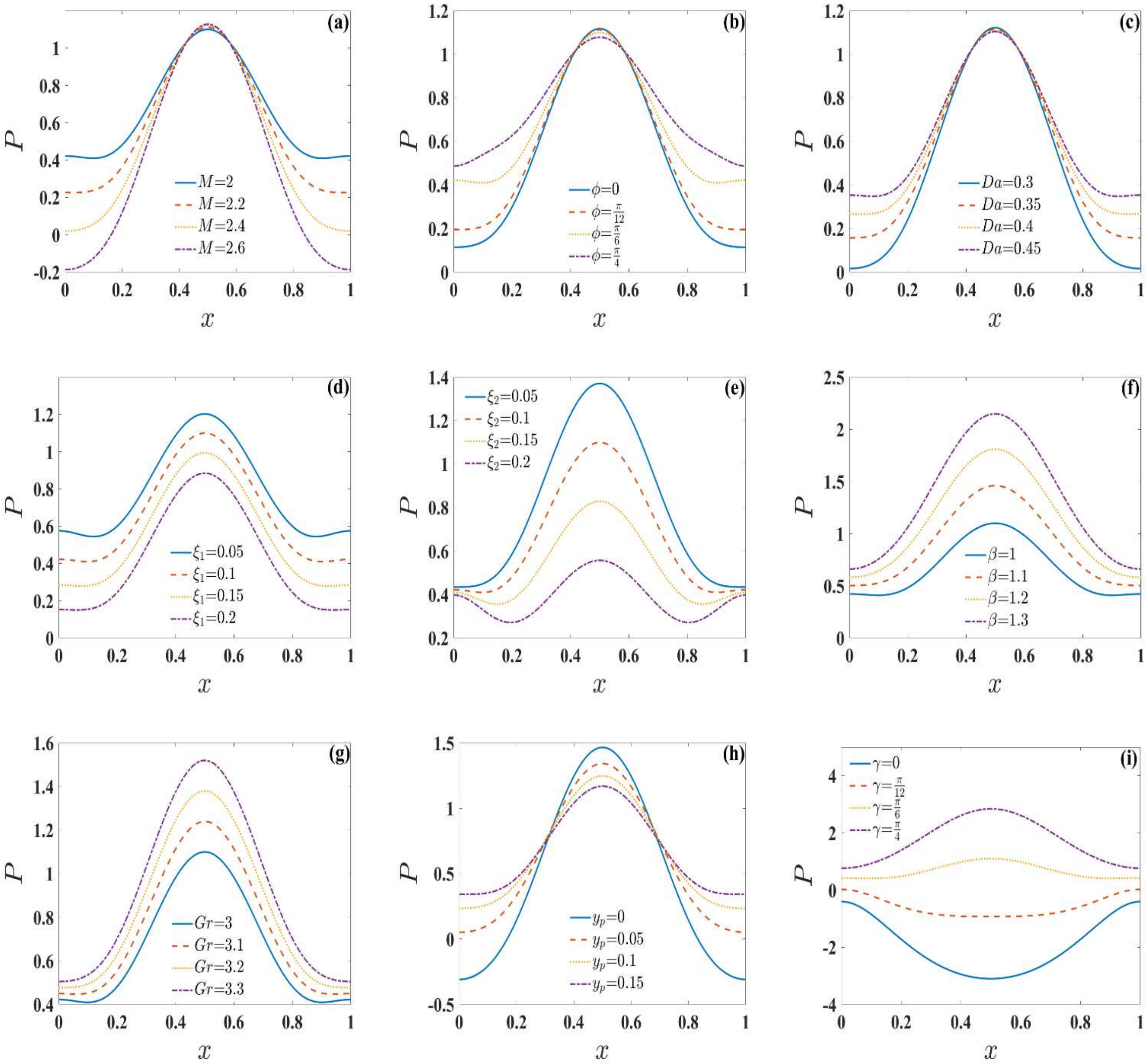

Fig. 4. Variation in the plots of pressure gradient for different values of (a) M, (b) ϕ, (c) Da, (d) ξ_1, (e) ξ_2, (f) β, (g) Gr, (h) y_p and (i) γ.

4.1 Heat Characteristics

Figure 2 shows the variation in temperature profiles for varying physical parameters. From the figure, it can be seen that the temperature profiles display a parabolic form, with the peak occurring in the central part of the channel. The significance of β on the temperature of the fluid is shown in Fig. 2(a), where it can be seen to have an increasing effect on temperature. In the flow of blood through arterioles, this behavior is reasonable due to the thickening of the boundary layer as heat is generated, which results in an appreciable rise in the layer temperature. An opposite behavior is observed for increasing values of Bi (see Fig. 2(b)). However, Fig. 2(c) shows an enhancement in the fluid temperature with the increasing variable thermal conductivity.
The nature of heat transfer coefficient Z is graphed in Fig. 3. Due to sinusoidal wave behavior, it suffices to consider the graph over only one wavelength. For demonstration purpose, we have considered the wavelength over the interval [0, 1]. Moreover, it can be noticed that Z changes its sign from the left to the right of the mean value 0.5. It can be observed that the peristaltic waves define the oscillatory action of the heat transfer coefficient. Also, from Fig. 3(a), it can be noticed that the amplitude of these oscillations increase with the values of β. A similar nature of Z is seen in Fig. 3(b) for increasing values of Bi. The maximum value of Z is found to decrease for higher values of ξ_2 and smaller values of ε (see Figs. 3(c) and 3(d)).

4.2 Pumping Characteristics

This subsection attempts to describe the pressure gradient, pressure rise and frictional force for various pertinent parameters through graphs plotted in Figs. 4 - 6. The pressure gradient is plotted against the axial distance in Fig. 4. It is interesting to notice that for $x \in [0,0.3]$ and $x \in [0.3,1]$, not much pressure gradient needs to be imposed for the fluid to flow easily, whereas for $x \in [0.3,0.6]$, especially $x = 0.5$, the required pressure gradient is comparatively higher to regulate the same fluid flux to pass through. From Fig. 4(a), it can be seen that as the magnetic field becomes stronger, the pressure gradient is seen to increase in the central portion of the channel. This observation suggests the importance of the strength of the magnetic field that can be applied to regulate the flow. Hence, it finds applications in the field of medicine and surgery where a magnetic field of suitable strength can be used to control excessive bleeding. The influence of the angle in which the magnetic field is applied, ϕ can be observed in Fig. 4(b). As the magnetic field increases in inclination, a reduction in the pressure gradient is observed in the central part. However, on the contrary, the influence of porosity of the medium is depicted in Fig. 4(c), wherein, the pressure gradient needed to maintain the same fluid flux through the channel in its center decreases with increasing porosity. Figures 4(d)-4(e) show that the variable viscosity ξ_1 as well as thermal conductivity ξ_2 have a decreasing effect on the pressure gradient. The increasing values of β and Gr are seen to increase the pressure gradient in the channel (see Figs. 4(f)-4(g)). Figures 4(h)-4(i) are plotted for the impacts of y_p and γ on the pressure gradient.

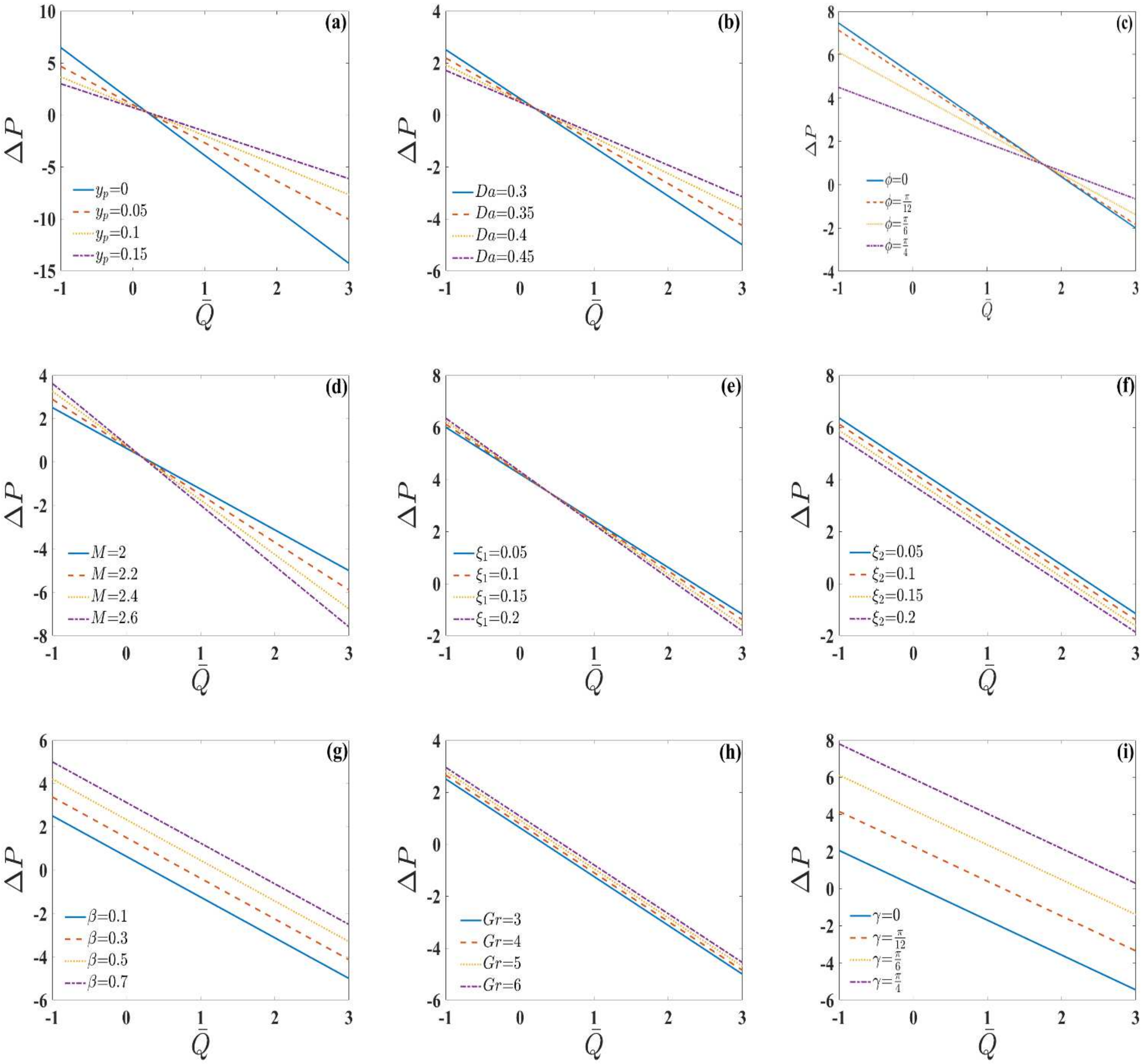

Fig. 5. Variation in the plots of pressure rise for different values of (a) y_p, (b) Da, (c) ϕ, (d) M, (e) ξ_1, (f) ξ_2, (g) β, (h) Gr and (i) γ.

Plots for pressure rise per wavelength ΔP_λ versus the volumetric flow rate $\bar{Q}$ is shown in Fig. 5. This property of peristaltic pumping in opposition to the pressure rise is significant to the peristaltic study. The plane of graph can be divided into four regions, namely peristaltic pumping, free pumping, retrograde pumping and augmented pumping/co-pumping regions. For the free pumping region, $\Delta P_\lambda = 0$ and the fluid flow occurs solely by the peristaltic movement of the walls. The peristaltic pumping region of the graph is where $\Delta P_\lambda > 0$ and $\bar{Q} > 0$. In this region, the fluid flows in the forward direction after the peristalsis of the walls overcome the resistance offered by the pressure gradient. When $\Delta P_\lambda > 0$ and $\bar{Q} < 0$, we have the region of retrograde pumping, where fluid flows opposite to that of the peristaltic waves and the flow happens due to the pressure gradient. In the augmented pumping region, $\Delta P_\lambda < 0$ and $\bar{Q} > 0$. The negative pressure gradient of this region aids the fluid flow caused by the peristaltic motion of the walls. The influence of y_p, Da and ϕ are depicted in Figs. 5(a)-5(c). It can be noticed that these parameters increase the pumping rate in the retrograde region and decrease it in the augmented region. However, in the peristaltic region, a decrease in the pumping rate can be seen till a critical value of $\bar{Q}$, and increases thereafter. A trend opposite to this is observed in Figs. 5(d)-5(e) for Hartmann number M and variable viscosity parameter ξ_1. However, for increasing values of ξ_2, the pumping rate decreases significantly in augmented, peristaltic as well as retrograde pumping regions (see Fig. 5(f)). Figures 5(g)-5(i) show that the rate of pumping across all regions rises for higher values of β, Gr and γ. To observe the impacts of the various parameters on the plots of frictional force versus the flow rate, we have Fig. 6. These plots indicate that when compared to pressure rise, frictional forces have an exactly opposite behavior.

4.3 Trapping Phenomenon

A study of the trapping phenomenon is an integral part of the peristaltic mechanism. During peristalsis, few of the streamlines get closed, resulting in the formation of bolus which circulates internally and moves forward with the speed of the peristaltic waves. This phenomenon is called trapping. Few important typical physical examples include the formation of food bolus in the gastrointestinal tract and thrombus in the blood. This section attempts to study this interesting phenomenon of trapping through the plots of streamline function. Figure 7 gives the pictorial representation of the variation in bolus formation for varying M. A reduction in the bolus size is clearly seen as the value of M increases. Similar observation is made in Fig. 8 for increasing values of Gr. However, the porous parameter Da is seen to increase the size of the bolus trapped during peristalsis (see Fig. 9). To study the influence of variable viscosity on the bolus size, Fig. 10 is plotted, in which it can be noticed that ξ_1 contributes to a decrease in the bolus size.

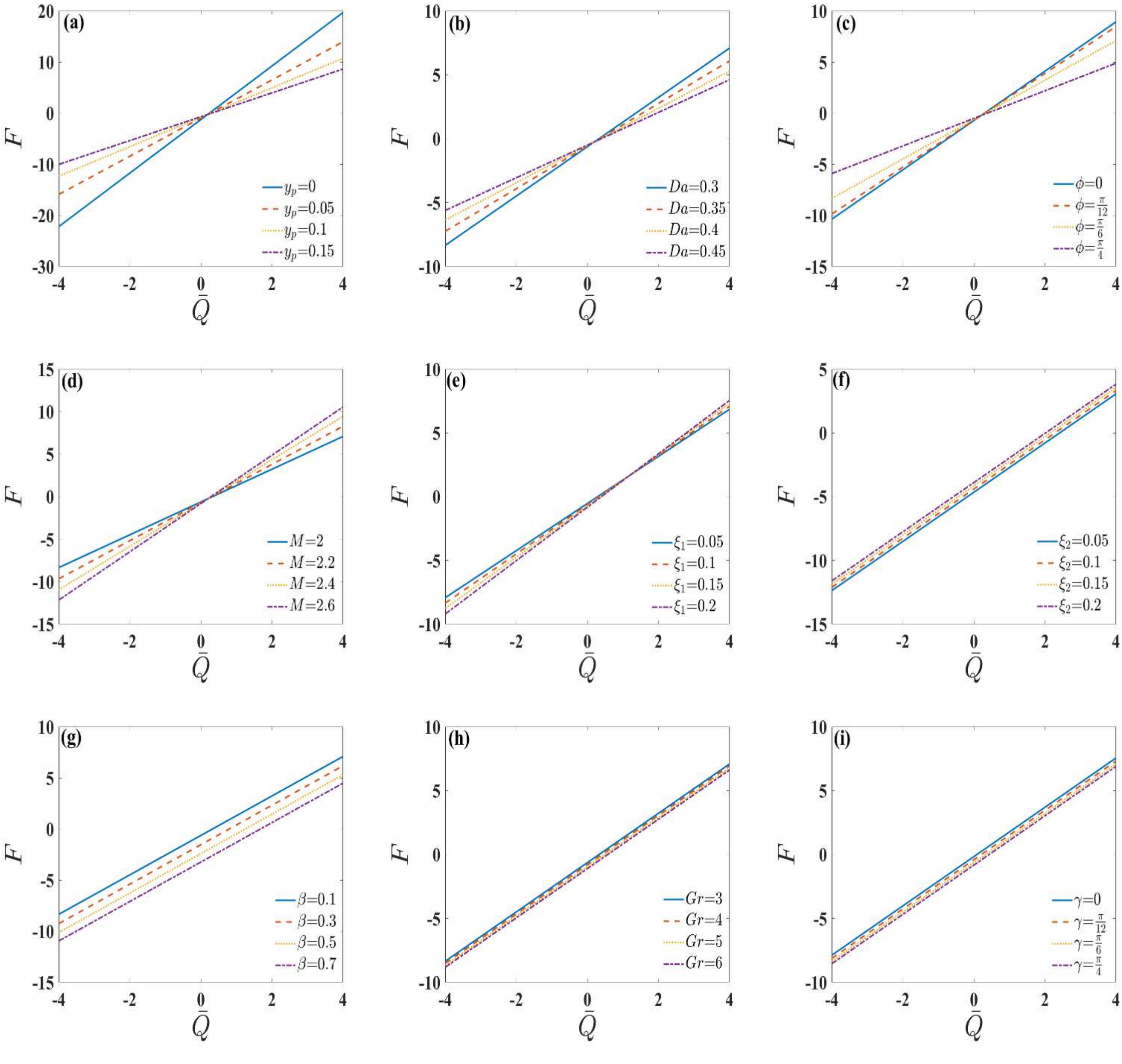

Fig. 6. Variation in the plots of frictional force for different values of (a) y_p, (b) Da, (c) ϕ, (d) M, (e) ξ_1, (f) ξ_2, (g) β, (h) Gr and (i) γ.

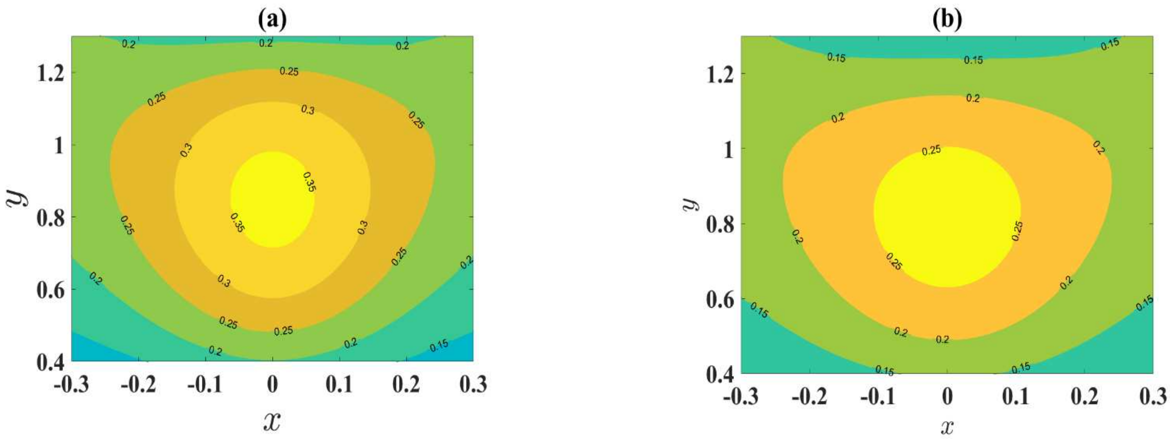

Fig. 7. Streamlines for (a) $M = 2$ and (b) $M = 2.2$.

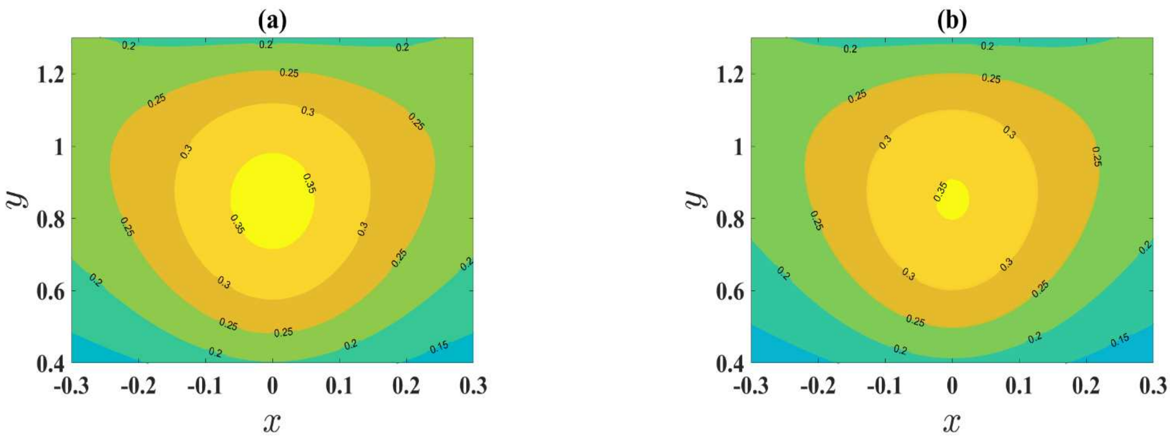

Fig. 8. Streamlines for (a) $Gr = 3$ and (b) $Gr = 3.1$.

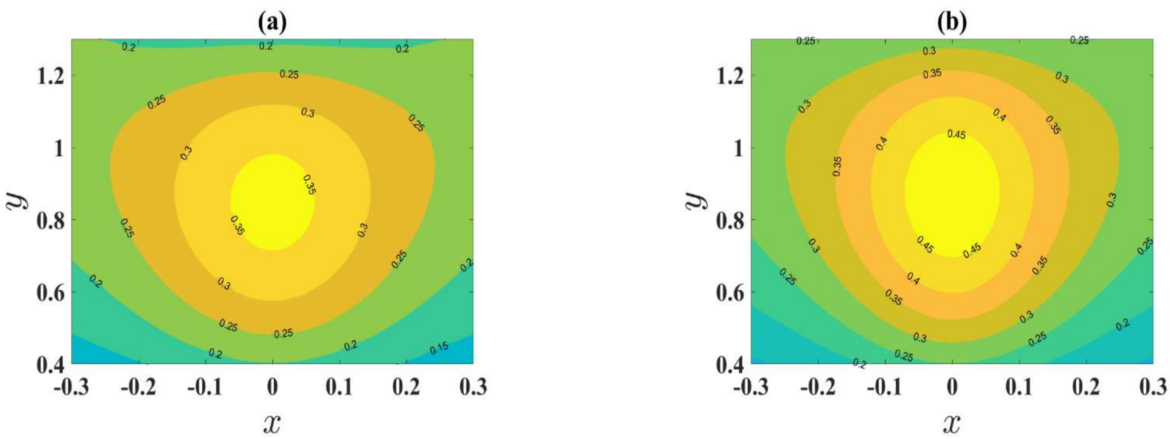

Fig. 9. Streamlines for (a) $Da = 0.3$ and (b) $Da = 0.35$.

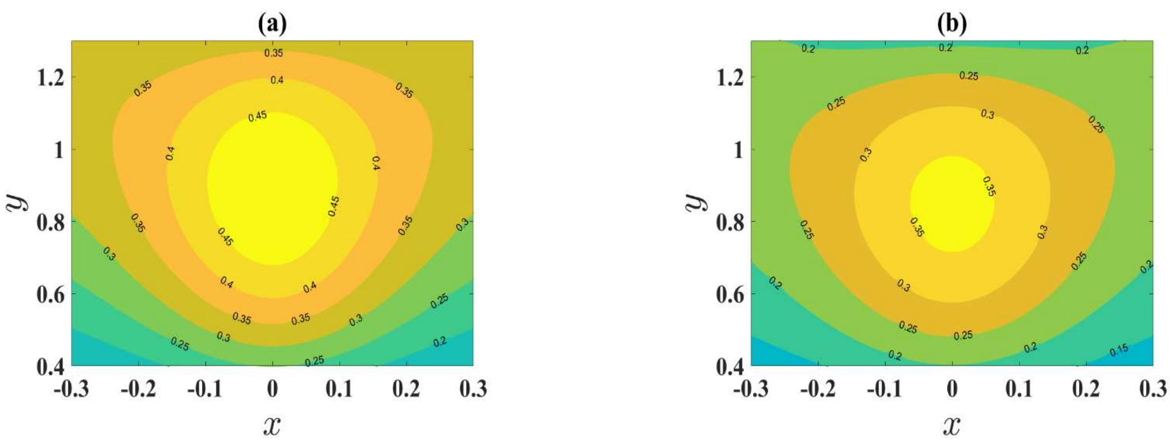

Fig. 10. Streamlines for (a) $\xi_1 = 0.05$ and (b) $\xi_1 = 0.1$.

5. Conclusions

The work done in this article intends to investigate the impact of variable thermal conductivity and convective boundary conditions on the transfer of heat within a Bingham fluid possessing a variation in viscosity. The fluid flows through a porous medium and is exposed to an inclined magnetic field. The two-dimensional channel through which the fluid flows is considered to be inclined at a certain angle with the horizontal surface. The results for a horizontal channel and magnetic field can be obtained by considering $\gamma = 0$ and $\phi = 0$ respectively. The governing equations are solved for temperature and velocity by the semi-analytical technique of perturbation for small values of ξ_1 (variable viscosity) and ξ_2 (variable thermal conductivity). The pressure rise and frictional force are numerically evaluated using MATLAB. The results obtained in the present study are in good agreement with those of Rathod and Laxmi [28]. The functioning of heart lung and dialysis machines depend on the mechanism of peristaltic pumping. The results of the current work help in determining the variation required in the parameters like M, Da, ϕ and γ so as to create/maintain a particular pressure rise or pressure gradient. Few of the important results are as follows:

- Higher values of Biot number decreases the temperature of the fluid but increases the oscillations of the heat transfer coefficient.
- An increase in the variable thermal conductivity rises the fluid temperature and lowers the heat transfer coefficient.
- Pumping rate increases for Grashof number, magnetic parameter and variable viscosity.
- Best pumping is obtained for lower values of Darcy number and variable thermal conductivity.
- Pumping performance is better for inclined channel and non-inclined magnetic field.
- Frictional force and pressure rise behave in opposite ways.
- The size of the trapped bolus reduces for higher values of magnetic parameter and variable viscosity.
- The porous parameter aids in increasing the size of bolus formed during trapping.

Author Contributions

B.B. Divya identified and planned the topic for investigation; G. Manjunatha developed the mathematical modeling and examined the theory of validation; C. Rajashekhar carried out the solution procedure; H. Vaidya and K.V. Prasad conducted the parametric analysis and interpretation of the results. The manuscript was written through the contribution of all authors. All authors discussed the results, reviewed and approved the final version of the manuscript.

Conflict of Interest

The authors declared no potential conflicts of interest with respect to the research, authorship and publication of this article.

Funding

The authors received no financial support for the research, authorship and publication of this article.

Nomenclature

a'	Undeformed radius of the channel	y_p	Radius of plug flow region
b'	Wave amplitude	***Greek symbols***	
B_0	Strength of magnetic field	β	Heat generation parameter
c	Wave speed	β'	Linear thermal expansion parameter
c_p	Specific heat at constant pressure	ε	Amplitude ratio
Da	Porosity parameter (Darcy number)	δ	Wave number
g	Acceleration due to gravity	γ	Angle of inclination of the channel
Gr	Grashof number	$\dot{\gamma}_{ij}$	Strain tensors
k^*	Thermal conductivity of the fluid	λ	Wavelength
M	Magnetic parameter (Hartmann number)	$\mu(y)$	Varying fluid viscosity
p	Pressure	ϕ	Angle of inclination of the magnetic field
Pr	Prandtl number	ψ	Streamline function
Q_0	Constant heat absorption or addition	ρ	Constant fluid density
Re	Reynolds number	σ	Electrical conductivity of the fluid
t	Time	τ_{ij}	Stress tensors
v	Radial velocity	τ_0	Yield stress
w	Axial velocity	θ	Non-dimensional temperature
x	Non-dimensional axial distance	ξ_1	Coefficient of variable viscosity
y	Non-dimensional radial distance	ξ_2	Coefficient of variable thermal conductivity

References

[1] Srivastava, L.M., Srivastava, V.P., Peristaltic transport of a non-Newtonian fluid: applications to the vas deferens and small intestine. *Annals of Biomedical Engineering*, 13(2), 1985, 137-153.
[2] Narahari, M., Sreenadh, S., Peristaltic transport of a Bingham fluid in contact with a Newtonian fluid. *International Journal of Applied Mathematics and Mechanics*, 6(11), 2010, 41-54.
[3] Frigaard, I.A., Ryan, D.P., Flow of a visco-plastic fluid in a channel of slowly varying width. *Journal of Non-Newtonian Fluid Mechanics*, 123(1), 2004, 67-

83.
[4] Fusi, L., Non-isothermal flow of a Bingham fluid with pressure and temperature dependent viscosity. *Meccanica*, 52(15), 2017, 3577-3592.
[5] Vaidya, H., Rajashekhar, C., Manjunatha, G., Prasad, K.V., Effects of Heat Transfer on Peristaltic Transport of a Bingham Fluid through an Inclined Tube with Different Wave Forms. *Defect and Diffusion Forum*, 392, 2019, 158-177.
[6] Vaidya, H., Rajashekhar, C., Manjunatha, G., Prasad, K.V., Rheological properties and peristalsis of Rabinowitsch fluid through compliant porous walls in an inclined channel. *Journal of Nanofluids*, 8(5), 2018, 970-979.
[7] Alkasassbeh, M., Omar, Z., Mebarek-Oudina, F., Raza, J., Chamkha, A.J., Heat transfer study of convective fin with temperature-dependent internal heat generation by hybrid block method. *Heat Transfer—Asian Research*, 48(4), 2019, 1225-1244.
[8] Mebarek-Oudina, F., Bessaïh, R., Numerical simulation of natural convection heat transfer of copper-water nanofluid in a vertical cylindrical annulus with heat sources. *Thermophysics and Aeromechanics*, 26(3), 2019, 325-334.
[9] Shamshuddin, M.D., Thirupathi, T., Satya Narayana, P.V., Micropolar Fluid Flow Induced due to a Stretching Sheet with Heat Source/Sink and Surface Heat Flux Boundary Condition Effects. *Journal of Applied and Computational Mechanics*, 5(5), 2019, 816-826.
[10] Abdelsalam, S.I., Bhatti, M.M., The study of non-Newtonian nanofluid with hall and ion slip effects on peristaltically induced motion in a non-uniform channel. *RSC Advances*, 8(15), 2018, 7904-7915.
[11] Akram, S., Nadeem, S., Hussain, A., Effects of heat and mass transfer on peristaltic flow of a Bingham fluid in the presence of inclined magnetic field and channel with different wave forms. *Journal of Magnetism and Magnetic Materials*, 362, 2014, 184-192.
[12] Sinha, A., Shit, G.C., Ranjit, N.K., Peristaltic transport of MHD flow and heat transfer in an asymmetric channel: Effects of variable viscosity, velocity-slip and temperature jump. *Alexandria Engineering Journal*, 54(3), 2015, 691-704.
[13] Akbar, N.S., Butt, A.W., Ferromagnetic effects for peristaltic flow of Cu–water nanofluid for different shapes of nanosize particles. *Applied Nanoscience*, 6(3), 2016, 379-385.
[14] Akbar, N.S., Butt, A.W., Ferromagnetic nano model study for the peristaltic flow in a plumb duct with permeable walls. *Microsystem Technologies*, 25(4), 2019, 1227-1234.
[15] Hayat, T., Hina, S., The influence of wall properties on the MHD peristaltic flow of a Maxwell fluid with heat and mass transfer. *Nonlinear analysis: Real World Applications*, 11(4), 2010, 3155-3169.
[16] Hayat, T., Bibi, S., Rafiq, M., Alsaedi, A., Abbasi, F.M., Effect of an inclined magnetic field on peristaltic flow of Williamson fluid in an inclined channel with convective conditions. *Journal of Magnetism and Magnetic Materials*, 401, 2016, 733-745.
[17] Qasim, M., Ali, Z., Wakif, A., Boulahia, Z., Numerical Simulation of MHD Peristaltic Flow with Variable Electrical Conductivity and Joule Dissipation Using Generalized Differential Quadrature Method. *Communications in Theoretical Physics*, 71(5), 2019, 509.
[18] Abdelsalam, S.I., Vafai, K., Combined effects of magnetic field and rheological properties on the peristaltic flow of a compressible fluid in a microfluidic channel. *European Journal of Mechanics-B/Fluids*, 65, 2017, 398-411.
[19] Wakif, A., Boulahia, Z., Ali, F., Eid, M.R., Sehaqui, R., Numerical analysis of the unsteady natural convection MHD couette nanofluid flow in the presence of thermal radiation using single and two-phase nanofluid models for Cu–Water nanofluids. *International Journal of Applied and Computational Mathematics*, 4(3), 2018, 81.
[20] Hamrelaine, S., Mebarek-Oudina, F., Sari, M.R., Analysis of MHD Jeffery Hamel flow with suction/injection by homotopy analysis method. *Journal of Advanced Research in Fluid Mechanics and Thermal Sciences*, 58, 2019, 173-186.
[21] Akbar, N.S., Butt, A.W., Entropy generation analysis for the peristaltic flow of Cu-water nanofluid in a tube with viscous dissipation. *Journal of Hydrodynamics*, 29(1), 2017, 135-143.
[22] Kothandapani, M., Srinivas, S., On the influence of wall properties in the MHD peristaltic transport with heat transfer and porous medium. *Physics Letters A*, 372(25), 2008, 4586-4591.
[23] Srinivas, S., Gayathri, R., Peristaltic transport of a Newtonian fluid in a vertical asymmetric channel with heat transfer and porous medium. *Applied Mathematics and Computation*, 215(1), 2009, 185-196.
[24] Srinivas, S., Gayathri, R., Kothandapani, M., The influence of slip conditions, wall properties and heat transfer on MHD peristaltic transport. *Computer Physics Communications*, 180(11), 2009, 2115-2122.
[25] Eldesoky, I.M., Abdelsalam, S.I., El-Askary, W.A., Ahmed, M.M., Concurrent Development of Thermal Energy with Magnetic Field on a Particle-Fluid Suspension through a Porous Conduit. *BioNanoScience*, 9(1), 2019, 186-202.
[26] Ramesh, K., Devakar, M., Magnetohydrodynamic peristaltic transport of couple stress fluid through porous medium in an inclined asymmetric channel with heat transfer. *Journal of Magnetism and Magnetic Materials*, 394, 2015, 335-348.
[27] Mahmoud, S.R., Afifi, N.A.S., Al-Isede, H.M., Effect of porous medium and magnetic field on peristaltic transport of a Jeffrey fluid. *International Journal of Mathematical Analysis*, 5, 2011, 1025-1034.
[28] Rathod, V.P., Laxmi, D., Effects of heat transfer on the peristaltic MHD flow of a Bingham fluid through a porous medium in a channel. *International Journal of Biomathematics*, 7(6), 2014, 1450060.
[29] Lakshminarayana, P., Sreenadh, S., Sucharitha, G., The influence of slip, wall properties on the peristaltic transport of a conducting Bingham fluid with heat transfer. *Procedia Engineering*, 127, 2015, 1087-1094.
[30] Wakif, A., Boulahia, Z., Sehaqui, R., Analytical and numerical study of the onset of electroconvection in a dielectric nanofluid saturated a rotating Darcy porous medium. *International Journal of Advanced Computer Science & Applications*, 7, 2016, 299-311.
[31] Rajesh, R., Rajasekhara Gowd, Y., Heat and Mass Transfer Analysis on MHD Peristaltic Prandtl Fluid Model through a Tapered Channel with Thermal Radiation. *Journal of Applied and Computational Mechanics*, 5(5), 2019, 951-963.
[32] Sarkar, S., Endalew, M.F., Makinde, O.D., Study of MHD Second Grade Flow through a Porous Microchannel under the Dual-Phase-Lag Heat and Mass Transfer Model. *Journal of Applied and Computational Mechanics*, 5(4), 2019, 763-778.
[33] Mekheimer, K.S., Komy, S.R., Abdelsalam, S.I., Simultaneous effects of magnetic field and space porosity on compressible Maxwell fluid transport induced by a surface acoustic wave in a microchannel. *Chinese Physics B*, 22(12), 2013, 124702.
[34] Nadeem, S., Akbar, N.S., Effects of heat transfer on the peristaltic transport of MHD Newtonian fluid with variable viscosity: application of Adomian decomposition method. *Communications in Nonlinear Science and Numerical Simulation*, 14(11), 2009, 3844-3855.
[35] Manjunatha, G., Rajashekhar, C., Vaidya, H., Prasad, K.V., Simultaneous Effects of Heat Transfer and Variable Viscosity on Peristaltic Transport of Casson Fluid Flow in an Inclined Porous Tube. *International Journal of Applied Mechanics and Engineering*, 24(2), 2019, 309-328.
[36] Fusi, L., Farina, A., Rosso, F., Retrieving the Bingham model from a bi-viscous model: some explanatory remarks. *Applied Mathematics Letters*, 27, 2014, 11-14.
[37] Manjunatha, G., Rajashekhar, C., Vaidya, H., Prasad, K.V., Peristaltic mechanism of Bingham liquid in a convectively heated porous tube in the presence of variable liquid properties. *Special Topics & Reviews in Porous Media: An International Journal*, 10(2), 2019, 1-10.
[38] Vaidya, H., Rajashekhar, C., Manjunatha, G., Prasad, K.V., Effect of variable liquid properties on peristaltic flow of a Rabinowitsch fluid in an inclined convective porous channel. *The European Physical Journal Plus*, 134(5), 2019, 231.
[39] Divya, B., Manjunatha, G., Rajashekhar, C., Hanumesh, V., Prasad, K., Impact of variable liquid properties on Peristaltic mechanism of convectively heated Jeffrey fluid in a slippery elastic tube. *Frontiers in Heat and Mass Transfer*, 12, 2018, 15.

Appendix

$$c_2 = \frac{\beta}{Bi}\left(h + Bi\frac{h^2}{2}\right), \tag{A1}$$

$$c_3 = \frac{1}{Bi}\left[\left(\frac{-\beta h^2}{2} + c_2\right)\left(-\beta h + \frac{Bi}{2}\left(-\beta\frac{h^2}{2} + c_2\right)\right)\right], \tag{A2}$$

$$c_4 = \frac{1}{E^2 \cos Eh}\left[P - c_5 E^2 \sin Eh - Gr\sin\gamma\left(c_6 + \beta\left(c_7 + c_8 h^2 - \frac{\xi_2\beta}{8}\left(h^4 - \frac{12h^2}{E^2} + \frac{24}{E^4}\right)\right)\right)\right], \tag{A3}$$

$$c_5 = \frac{\tau_0}{E},\ c_6 = c_2 + \xi_2 c_3 - \frac{\xi_2 c_2^2}{2},\ c_7 = \frac{-\xi_2 c_2 + 1}{E^2},\ c_8 = \frac{\xi_2 c_2 - 1}{2}, \tag{A4}$$

$$c_9 = \frac{1}{\cos Eh}\left[-1 - c_{10}\sin Eh - \frac{Eh^2}{4}(c_5\cos Eh - c_4 \sin Eh) - \frac{h}{4}(c_5 \sin Eh + c_4\cos Eh) - \frac{Gr\beta\sin\gamma}{E^4}\left(4c_8 h + \frac{18\xi_2\beta h}{E^2} - 2\xi_2\beta h^3\right)\right], \tag{A5}$$

$$c_{10} = \frac{1}{E}\left[\tau_0 - \frac{c_4}{4} - \frac{Gr\beta\sin\gamma}{E^4}\left(4c_8 + \frac{18\xi_2\beta}{E^2}\right)\right], \tag{A6}$$

$$c_{11} = \frac{-Gr\sin\gamma}{E^2\cos Eh}\left[c_6 + \beta\left(c_7 + c_8 h^2 - \frac{\xi_2\beta}{8}\left(h^4 - \frac{12h^2}{E^2} + \frac{24}{E^4}\right)\right)\right], \tag{A7}$$

$$c_{12} = \frac{1}{E}\left[\frac{c_{11}}{4} + \frac{Gr\beta\sin\gamma}{E^4}\left(4c_8 + \frac{18\xi_2\beta}{E^2}\right)\right], \tag{A8}$$

$$c_{13} = c_{11}\left(\frac{Eh^2\tan Eh}{4} - \frac{h}{4}\right) + \frac{1}{\cos Eh}\left[-1 + c_{12}\sin Eh - \frac{Gr\beta\sin\gamma}{E^4}\left(4c_8 h + \frac{18\xi_2\beta h}{E^2} - 2\xi_2\beta h^3\right)\right], \tag{A9}$$

$$c_{14} = 4c_8 + \frac{18\xi_2\beta}{E^2}, \tag{A10}$$

$$c_{15} = \tan Eh\left(1 + \frac{3\xi_1 y_p}{4}\right) + \xi_1\left(\frac{E}{4}\left(h^2 - y_p^2\right) + \tan Eh + \frac{1 + \tan^2 Eh}{4E} + \frac{Eh^2\tan^2 Eh}{4}\right), \tag{A11}$$

$$c_{16} = 1 + \xi_1 + \frac{\xi_1 y_p}{4}\left(3 + Ey_p \tan Eh\right), \tag{A12}$$

$$c_{17} = \frac{\sec Eh\left[E\sin Ey_p\left(1 + \frac{3\xi_1 y_p}{4}\right) - \frac{\cos Ey_p}{4}\left(\xi_1 - \xi_1 E^2 y_p^2\right)\right]}{E^2\left(c_{15}\sin Ey_p + c_{16}\cos Ey_p\right)}, \tag{A13}$$

$$\begin{aligned} c_{18} = \frac{1}{4E^4\left(c_{15}\sin Ey_p + c_{16}\cos Ey_p\right)}\Big[E^4\Big[\xi_1\cos Ey_p\left(4Ec_{12} + c_{11}\left(-1 + E^2 y_p^2\right)\right) + E\sin Ey_p\left(4\xi_1 c_{13} + c_{11}\left(4 + 3\xi_1 y_p\right)\right)\Big] + \\ 2Gr\beta\sin\gamma\left(-2E^2\left(2c_8 y_p + c_{14}\xi_1\right) + \xi_2\beta y_p\left(-6 + E^2 y_p\left(y_p + 12\xi_1\right)\right)\right)\Big] \end{aligned} \tag{A14}$$

$$c_{19} = c_4 + \xi_1 c_9 + \frac{c_5 E y_p^2 \xi_1}{4} + \frac{c_4 y_p \xi_1}{4}, \tag{A15}$$

$$c_{20} = c_5 + \xi_1 c_{10} - \frac{c_4 E y_p^2 \xi_1}{4} + \frac{c_5 y_p \xi_1}{4}, \tag{A16}$$

$$c_{21} = \frac{\beta}{8}\left(y_p^4 - \frac{12 y_p^2}{E^2} + \frac{24}{E^4}\right), \tag{A17}$$

$$c_{22} = \frac{1}{E^2}\left(4c_8 y_p + \frac{18\xi_2\beta y_p}{E^2} - 2\xi_2\beta y_p^3\right), \tag{A18}$$

$$c_{23} = \xi_1\left(\frac{Eh^2}{4} + \tan Eh + \frac{Eh^2\tan^2 Eh}{4} + \frac{\tan^2 Eh}{4E}\right), \tag{A19}$$

$$c_{24} = c_{11}\left(1 + \frac{y_p\xi_1}{4}\right) + \xi_1 c_{13}, \tag{A20}$$

$$c_{25}=\frac{Ey_p^2\xi_1}{4}-\left(1+\frac{y_p\xi_1}{4}\right)\tan Eh-c_{23}, \tag{A21}$$

$$c_{26}=\frac{c_{17}y_p^2\xi_1}{4}-\frac{c_{17}\tan Eh}{E}\left(1+\frac{y_p\xi_1}{4}\right)-\frac{c_{17}c_{23}}{E}+\frac{\sec Eh}{E^2}\left[1+\frac{y_p\xi_1}{4}+\frac{\xi_1}{4E}\left(\tan Eh\left(1+E^2h^2\right)-Eh\right)\right], \tag{A22}$$

$$c_{27}=c_{24}-\frac{c_{18}c_{25}}{E},\quad c_{28}=\xi_1 c_{12}+\frac{Ey_p^2\xi_1 c_{11}}{4}, \tag{A23}$$

$$c_{29}=\frac{c_{17}}{E}\left[1+\frac{y_p\xi_1}{4}+\xi_1\left(1+\frac{\tan Eh}{4E}\right)+\frac{Ey_p^2\xi_1\tan Eh}{4}\right]-\frac{\xi_1\sec Eh}{4E^3}-\frac{y_p^2\xi_1\sec Eh}{4E}, \tag{A24}$$

$$c_{30}=\frac{c_{18}}{E}\left[1+\frac{y_p\xi_1}{4}+\xi_1\left(1+\frac{\tan Eh}{4E}\right)+\frac{Ey_p^2\xi_1\tan Eh}{4}\right], \tag{A25}$$

$$c_{31}=y_p c_{21}+\frac{\beta}{8}\left[\frac{\left(h-y_p\right)^5}{5}-\frac{4\left(h-y_p\right)^3}{E^2}+\frac{24\left(h-y_p\right)}{E^4}\right], \tag{A26}$$

$$c_{32}=y_p c_{22}+\frac{1}{E^2}\left[2c_8\left(h-y_p\right)^2+\frac{9\xi_2\beta\left(h-y_p\right)^2}{E^2}-\frac{\xi_2\beta\left(h-y_p\right)^4}{2}\right], \tag{A27}$$

$$c_{33}=\frac{1}{E}\left[c_4\left(1-\frac{\xi_1\left(h-y_p\right)}{2}\right)+c_5\left(\frac{\xi_1E\left(h-y_p\right)^2}{4}-\frac{\xi_1}{4E}\right)+\xi_1c_9\right], \tag{A28}$$

$$c_{34}=\frac{1}{E}\left[c_4\left(\frac{\xi_1E\left(h-y_p\right)^2}{4}-\frac{\xi_1}{4E}\right)+c_5\left(\frac{\xi_1\left(h-y_p\right)}{2}-1\right)+-\xi_1c_{10}\right], \tag{A29}$$

$$c_{35}=\frac{c_{11}}{E}\left(1-\frac{\xi_1\left(h-y_p\right)}{4}\right)+\frac{\xi_1c_{13}}{E}, \tag{A30}$$

$$c_{36}=-\tan Eh\left(1-\frac{\xi_1\left(h-y_p\right)}{4}\right)+\left(\frac{\xi_1E\left(h-y_p\right)^2}{4}-\frac{\xi_1}{4E}\right)-c_{23}, \tag{A31}$$

$$c_{37}=\frac{\sec Eh}{E^3}\left(1-\frac{\xi_1\left(h-y_p\right)}{4}\right)+\frac{\xi_1\sec Eh}{4E^4}\left(\left(1+E^2h^2\right)\tan Eh-Eh\right), \tag{A32}$$

$$c_{38}=\frac{c_{17}c_{36}}{E^2}+c_{37},\quad c_{39}=\frac{c_{18}c_{36}}{E^2}+c_{35}, \tag{A33}$$

$$c_{40}=\frac{c_{11}}{E}\left(\frac{\xi_1E\left(h-y_p\right)^2}{4}-\frac{\xi_1}{4E}\right)+\frac{\xi_1c_{12}}{E}, \tag{A34}$$

$$c_{41}=-\tan Eh\left(\frac{\xi_1E\left(h-y_p\right)^2}{4}-\frac{\xi_1}{4E}\right)+\left(\frac{\xi_1\left(h-y_p\right)}{4}-1\right)-\xi_1\left(1+\frac{\tan Eh}{4E}\right), \tag{A35}$$

$$c_{42}=\frac{\sec Eh}{E^3}\left(\frac{\xi_1E\left(h-y_p\right)^2}{4}-\frac{\xi_1}{4E}\right)+\frac{\xi_1}{4E^4}\sec Eh, \tag{A36}$$

$$c_{43}=\frac{c_{17}c_{41}}{E^2}+c_{42},\quad c_{44}=\frac{c_{18}c_{41}}{E^2}+c_{40}, \tag{A37}$$

$$c_{45} = \frac{Gr\sin\gamma}{E^2}\left[c_6 h + \beta\left(c_8\left(y_p^3 + \frac{(h-y_p)^3}{3}\right) + c_7 h - \xi_2 c_{31} + \xi_1 c_{32}\right)\right] \tag{A38}$$

ORCID iD

B.B. Divya http://orcid.org/0000-0001-9895-0634
G. Manjunatha http://orcid.org/0000-0001-5347-753X
C. Rajashekhar http://orcid.org/0000-0001-8950-7104
H. Vaidya http://orcid.org/0000-0001-5343-8039
K.V. Prasad http://orcid.org/0000-0001-6737-1162

How to cite this article: B.B. Divya, G. Manjunatha, C. Rajashekhar, H. Vaidya, K.V. Prasad, Effects of Inclined Magnetic Field and Porous Medium on Peristaltic Flow of a Bingham Fluid with Heat Transfer, *J. Appl. Comput. Mech.*, 7(4), 2021, 1892–1906. https://doi.org/10.22055/JACM.2019.31060.1822